

AFRL-PR-WP-TP-2006-205

**ADDITION OF NANOPARTICLE
DISPERSIONS TO ENHANCE FLUX
PINNING OF THE $\text{YBa}_2\text{Cu}_3\text{O}_{7-x}$
SUPERCONDUCTOR**



T. Haugan, P.N. Barnes, R. Wheeler, F. Meisenkothen, and M. Sumption

AUGUST 2004

Approved for public release; distribution is unlimited.

STINFO COPY

© 2004 Nature Publishing Group

This work is copyrighted. One or more of the authors is a U.S. Government employee working within the scope of their Government job; therefore, the U.S. Government is joint owner of the work and has the right to copy, distribute, and use the work. All other rights are reserved by the copyright owner.

**PROPULSION DIRECTORATE
AIR FORCE MATERIEL COMMAND
AIR FORCE RESEARCH LABORATORY
WRIGHT-PATTERSON AIR FORCE BASE, OH 45433-7251**

REPORT DOCUMENTATION PAGE

Form Approved
OMB No. 0704-0188

The public reporting burden for this collection of information is estimated to average 1 hour per response, including the time for reviewing instructions, searching existing data sources, gathering and maintaining the data needed, and completing and reviewing the collection of information. Send comments regarding this burden estimate or any other aspect of this collection of information, including suggestions for reducing this burden, to Department of Defense, Washington Headquarters Services, Directorate for Information Operations and Reports (0704-0188), 1215 Jefferson Davis Highway, Suite 1204, Arlington, VA 22202-4302. Respondents should be aware that notwithstanding any other provision of law, no person shall be subject to any penalty for failing to comply with a collection of information if it does not display a currently valid OMB control number. **PLEASE DO NOT RETURN YOUR FORM TO THE ABOVE ADDRESS.**

1. REPORT DATE (DD-MM-YY) August 2004		2. REPORT TYPE Journal Article Postprint		3. DATES COVERED (From - To) 08/19/2003 – 08/19/2004	
4. TITLE AND SUBTITLE ADDITION OF NANOPARTICLE DISPERSIONS TO ENHANCE FLUX PINNING OF THE YBa ₂ Cu ₃ O _{7-x} SUPERCONDUCTOR				5a. CONTRACT NUMBER In-house	
				5b. GRANT NUMBER	
				5c. PROGRAM ELEMENT NUMBER 61102F/62203F	
6. AUTHOR(S) T. Haugan, P.N. Barnes, R. Wheeler, and F. Meisenkothen (AFRL/PRPG) M. Sumption (The Ohio State University)				5d. PROJECT NUMBER 3145	
				5e. TASK NUMBER 32	
				5f. WORK UNIT NUMBER 314532Z9	
7. PERFORMING ORGANIZATION NAME(S) AND ADDRESS(ES) Power Generation Branch (AFRL/PRPG) Power Division Propulsion Directorate Air Force Research Laboratory, Air Force Materiel Command Wright-Patterson Air Force Base, OH 45433-7251				8. PERFORMING ORGANIZATION REPORT NUMBER AFRL-PR-WP-TP-2006-205	
9. SPONSORING/MONITORING AGENCY NAME(S) AND ADDRESS(ES) Propulsion Directorate Air Force Research Laboratory Air Force Materiel Command Wright-Patterson AFB, OH 45433-7251				10. SPONSORING/MONITORING AGENCY ACRONYM(S) AFRL-PR-WP	
				11. SPONSORING/MONITORING AGENCY REPORT NUMBER(S) AFRL-PR-WP-TP-2006-205	
12. DISTRIBUTION/AVAILABILITY STATEMENT Approved for public release; distribution is unlimited.					
13. SUPPLEMENTARY NOTES Journal article published in Nature, Vol. 430, 19 August 2004, Nature Publishing Group, publisher. PAO case number: ASC 04-0954; Date cleared: 06 Apr 2004. © 2004 Nature Publishing Group. This work is copyrighted. One or more of the authors is a U.S. Government employee working within the scope of their Government job; therefore, the U.S. Government is joint owner of the work and has the right to copy, distribute, and use the work. All other rights are reserved by the copyright owner.					
14. ABSTRACT After the discovery of type-II HTS, focus is to develop these materials for power applications. One of the problems has been that magnetic flux is not completely expelled but rather contained within magnetic fluxons, whose motion stops larger supercurrents. It's known that the critical current of these materials can be enhanced by incorporating a high density of extended defects to act as pinning centres for the fluxons. YBa ₂ Cu ₃ O ₇ (YBCO or 123) is the most promising material for such applications at higher temperatures. Pinning is optimized when the size of the defects approaches the superconducting coherence length (~2-4nm for YBCO at temperatures ≤ 77 K) and when the areal number density of defects is of the order of (H/2) × 10 ¹¹ cm ⁻² , where H is the applied magnetic field in tesla. Such a high density has been hard to get by material-processing methods that keep a nanosize defect, except through irradiation. Here we report a method for achieving a dispersion of ~8-nm-sized nanoparticles in YBCO with a high number density, which increases critical current (at 77 K) by a factor of two to three for high magnetic fields.					
15. SUBJECT TERMS YBCO, nanoparticle, flux pinning, superconductors					
16. SECURITY CLASSIFICATION OF:			17. LIMITATION OF ABSTRACT: SAR	18. NUMBER OF PAGES 10	19a. NAME OF RESPONSIBLE PERSON (Monitor) Paul N. Barnes 19b. TELEPHONE NUMBER (Include Area Code) N/A
a. REPORT Unclassified	b. ABSTRACT Unclassified	c. THIS PAGE Unclassified			

Addition of nanoparticle dispersions to enhance flux pinning of the $\text{YBa}_2\text{Cu}_3\text{O}_{7-x}$ superconductor

T. Haugan¹, P. N. Barnes¹, R. Wheeler¹, F. Meisenkothen¹ & M. Sumpston²

¹Air Force Research Laboratory, Wright-Patterson AFB, Ohio 45433-7919, USA

²Department of Materials Science and Engineering, The Ohio State University, Columbus, Ohio 43210, USA

Following the discovery of type-II high-temperature superconductors in 1986 (refs 1, 2), work has proceeded to develop these materials for power applications. One of the problems, however, has been that magnetic flux is not completely expelled, but rather is contained within magnetic fluxons, whose motion prevents larger supercurrents. It is known that the critical current of these materials can be enhanced by incorporating a high density of extended defects to act as pinning centres for the fluxons^{3,4}. $\text{YBa}_2\text{Cu}_3\text{O}_7$ (YBCO or 123) is the most promising material for such applications at higher temperatures (liquid nitrogen)³⁻¹³. Pinning is optimized when the size of the defects approaches the superconducting coherence length ($\sim 2-4$ nm for YBCO at temperatures ≤ 77 K) and when the areal number density of defects is of the order of $(H/2) \times 10^{11} \text{ cm}^{-2}$, where H is the applied magnetic field in tesla^{3,4}. Such a high density has been difficult to achieve by material-processing methods that maintain a nanosize defect, except through irradiation⁵. Here we report a method for achieving a dispersion of ~ 8 -nm-sized nanoparticles in YBCO with a high number density, which increases the critical current (at 77 K) by a factor of two to three for high magnetic fields.

The flux pinning enhancement of type II superconductors with defects have been studied in both copper-oxide high- and low-temperature superconductor materials^{3,4,14}. An areal number density of second-phase defects of over 10^{11} cm^{-2} was previously

achieved in NbTi type II low-temperature superconductors to increase the critical current, J_c (ref. 14). Dislocations are one class of defects in YBCO (hereafter referred to as 123) reportedly achieved in thin films with densities varying from 10^9 – 10^{11} cm^{-2} , depending on the deposition parameters^{15,16}. Dislocations were shown to be directly responsible for pinning in thin films¹⁵, but their density is still less than what is desired for complete flux pinning in the regimes of 2–6 T (refs 15, 16). To our knowledge, a density of second-phase defects exceeding 10^{10} cm^{-2} has not yet been achieved for YBCO. In addition to high defect density, it is desirable to minimize the defect size, which maximizes the superconducting volume and allows a higher areal defect density to be reached.

In this work, second-phase YBa_2CuO_5 (hereafter referred to as 211) particles of nanometre size were introduced by growth of alternating multilayers of ultrathin 211 and 123. Microscopy studies in Figs 1 and 2 reveal a near-uniform dispersion of second phase 211 nanoparticles grown by the island-growth mode in YBCO, demonstrating consistent epitaxial growth of YBCO around the 211 islands for up to 200 bilayers. The island-growth mechanism is expected for the $(211/123) \times N$ multilayer system, where N is the number of bilayers, because the lattice mismatch of 211 with respect to 123 is of the order of 2%–7%, depending on the growth orientation of 211 with respect to 123. For one film analysed with electron selected area diffraction, the growth orientation was 211 b axis//123 c axis, and the lattice mismatches calculated from reference patterns were, for lattice constants a , b and c : $a_{211}/2 \times (a,b)_{\text{avg}123} = -7.4\%$, where $(a,b)_{\text{avg}123}$ is the average of a and b in 123; $c_{211, \text{rip-45}^\circ}/(a,b)_{\text{avg}123} = +4.5\%$, where $c_{211, \text{rip-45}^\circ}$ is c rotated 45° in the plane; and $b_{211}/c_{123} = +4.5\%$. Other growth orientations might be possible, but they have not yet been observed. A large lattice mismatch favours the growth of island nanoparticles, because deposition is preferred on energetically favourable island-nucleated phases rather than the lattice-mismatched substrate or base layer¹⁷.

As shown in Fig. 2, the growth of $(211\text{-nanoparticle}/123\text{-film}) \times N$ multilayer films produced a superlattice-type structure with the 211 layers deposited as nanoparticles rather than homogeneous epitaxial layers. A repeating (nanoparticle/film) structure has been achieved with semiconductor materials that are described as three-dimensional quantum-dot or binary superlattices or crystals^{18–20}; however, to our knowledge, this type of structure has only been recently explored by our group in superconductors with initial experiments testing the $(211/123) \times N$ structure with N bilayers up to 100 (ref. 21). An advantage of the $(211/123) \times N$ structure for flux pinning is that it is possible to have some degree of control over the nanoparticle dispersion parameters, for example, by changing the 211 deposition conditions and varying the 123 layer thickness. These films can also provide a good experimental structure to test theories of flux pinning in high-temperature type II superconductors for uniform dispersions of point-like defects²².

Thin film samples were prepared by pulsed laser deposition (PLD) under conditions described previously²¹. Layers of 123 and 211 nanoparticles were deposited by ablation of separate 123 and 211 composition targets, using parameters chosen to optimize superconducting properties of the 123 phase²³. The O_2 deposition pressure was 300 mTorr. Unless noted otherwise, the composite films were deposited by computer program control of the laser and automated control of target movement. A delay of about 13 s was used between 123 and 211 depositions, during which the deposition was stopped and the targets were changed and moved into position. The plumes for 211 and 123 depositions were similar in size and shape, which allowed the use of the same PLD parameters. Substrates were LaAlO_3 or SrTiO_3 single crystals. The 123 layer and the 211 ‘pseudo-layer’ thicknesses were estimated by calibrating the deposition rates of both 123 and 211 for many depositions. These rates and the total sample thickness were used to calculate the

thicknesses of the 211 ‘pseudo-layer’ and 123 layer, assuming continuous coverage.

The formation of nanoparticles on the surfaces of films are shown in Fig. 1, as imaged with scanning electron microscopy (SEM). The nanoparticles are assumed to be insulating 211 phase, because the contrast seen for the particles is probably due to the insulating properties which cause charging and increased secondary electron emission. The nanoparticles were always observed on the film surfaces, with sizes and densities varying depending on 211 deposition parameters; typical particle sizes were 15 nm and particle densities about 1 – 1.3×10^{11} particles cm^{-2} , equivalent to a fluxon field of about 2–3 T, as shown in Fig. 1. Nanoparticles were observed to have diameters about twice as large on the surface as on the inside (as imaged with transmission electron microscopy (TEM) cross-sections). Assuming similar 211 area coverage for the surface and inside layers, the 211 densities inside the film are conservatively estimated as about four times higher, or $\sim(4\text{--}5) \times 10^{11}$ particles cm^{-2} . The actual number density may be higher, however, if the nanoparticle heights on the surface layers are also larger, which would increase the 211 volume. A similar calculation, using particle sizes and assuming the 211 layer achieves full coverage based on the calibrated deposition rate, indicates that the 211 densities might be as high as $(7\text{--}8) \times 10^{11}$ particles cm^{-2} . Therefore an initial estimate of the nanoparticle densities is $>4 \times 10^{11}$ particles cm^{-2} .

The increase of nanoparticle size on the surface also suggests the holding time at temperatures $>700^\circ\text{C}$ of the surface layer affects the 211 nucleation density and particle size, presumably by mechanisms of coalescence and ripening²⁰. Note that particle formation was especially enhanced on plateau edges and corners, which are expected to be energetically more favourable for coalescence sites¹⁷.

The formation of 211 nanoparticles was observed with cross-sectional TEM, as shown in Fig. 2. An important result of the TEM studies was that YBCO maintains a coherent structure as it grows around the 211 material. The uniform layering of the 211 phase can be clearly seen in Fig. 2a, which continued up to the surface of the $\sim 2\text{-}\mu\text{m}$ -thick film. The particle size and distribution are more clearly discerned in the bright-field transmission images in Fig. 2b

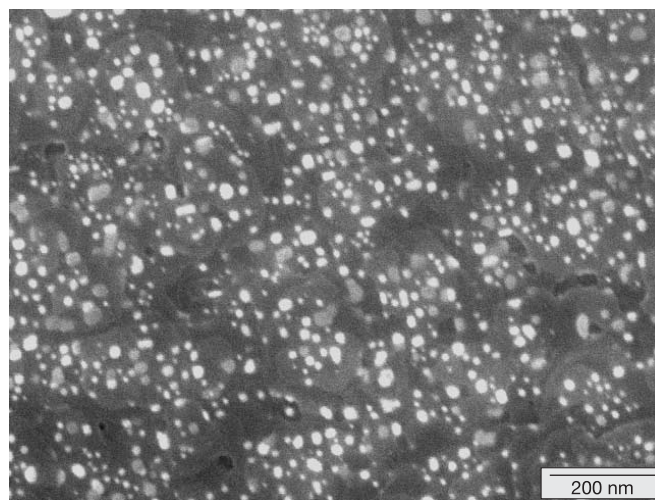


Figure 1 Micrograph of a YBCO + nanoparticle film showing surface nanoparticle formation. The image is from a $(211_{\sim 1.1 \text{ nm}}/123_{\sim 12.6 \text{ nm}}) \times 25$ multilayer film. White-image nanoparticles have average particle size 14.8 ± 0.7 nm and areal number density $\sim 1.1 \times 10^{11}$ particles cm^{-2} . Note that formation of nanoparticles occurred preferentially on the edges or corners of 123 ledges. Imaging was done with an SEM with 5 kV through a lens secondary detector in high-resolution mode, and imaging depth about 3 nm.

and c for different films. However, we note that TEM images provide a two-dimensional representation of particles embedded throughout the three-dimensional foil volume, and so the three-dimensional dispersion of particles is not yet precisely known. Similarly, the measured two-dimensional areal number density of nanoparticles for the films in Figs 2 and 3 ($\sim 5\text{--}6 \times 10^{11}$ particles cm^{-2}) cannot be used to calculate actual three-dimensional volumic or two-dimensional areal densities without knowing the precise foil thickness. For films in this study, the foil thickness was not measured at this time. The 211 particles are cross-sections of rectangular shape, surrounded by darker areas which can be considered a localized stress field that surrounds the particles²⁴.

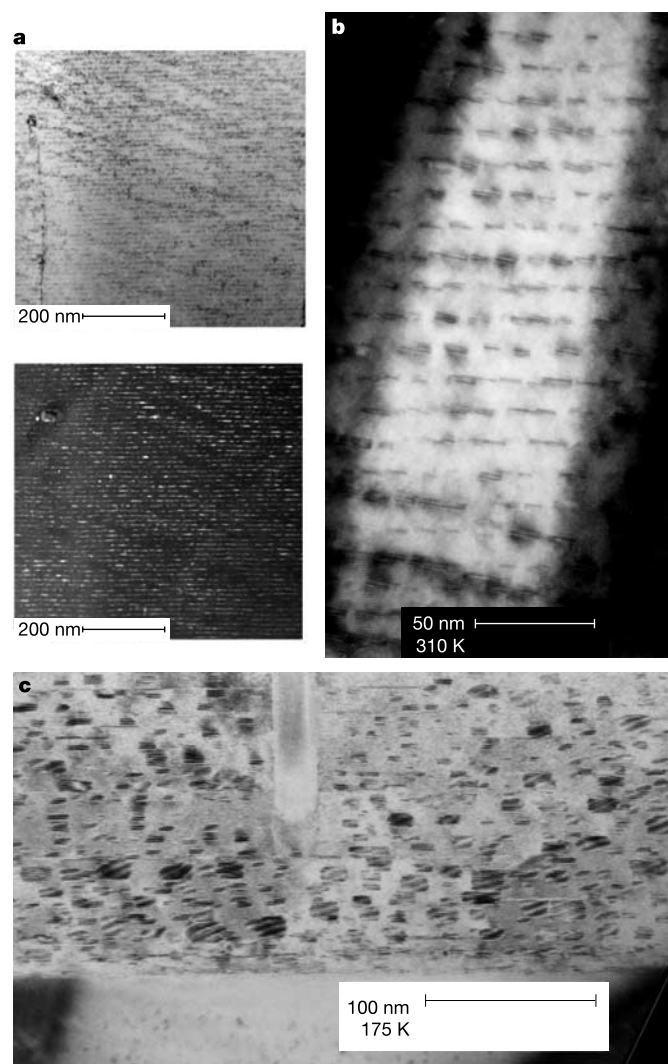


Figure 2 Transmission electron micrographs of YBCO + nanoparticle films, showing repeat layering structure and nanoparticle formations. Images are cross-sections of different films: **a**, **b**, $(211_{\sim 0.9 \text{ nm}}/123_{\sim 10.4 \text{ nm}}) \times 200$; **c**, $(211_{\sim 1.7 \text{ nm}}/123_{\sim 6.6 \text{ nm}}) \times 35$. **a**, A bright-field image (top) and a corresponding centred aperture dark-field image (bottom). The dark-field imaging conditions in **a** were established with a diffraction vector from the particle phase, thereby allowing the particle distribution to show up clearly against the 123 matrix phase. Nanoparticles are rectangular-shaped, about 8 nm in width in **b**, and 10–20 nm in width in **c**. Note the dislocation line in **a** and stress fields surrounding the 211 defects, and especially the formation of columnar-type defects in **b** and **c**, showing vertically stacked 211 connected by localized stress regions. The >100-nm-high vertically aligned defect is probably *a*-axis-oriented 123, which was only rarely observed in the multilayer films. The TEM for microscopy studies was a Philips CM-200 with a field-emission gun source.

These localized stress regions increase the size of the non-superconducting volume surrounding the defect, and thereby change the pinning properties.

As observed, especially in Fig. 2c, for a film with a thinner 123 layer spacing of ~ 6.5 nm, the localized stress region can extend between the nanoparticles that are vertically aligned, creating pseudo-columnar defects. For the sample in Fig. 2c, several growth mechanisms might have caused the more enhanced vertical alignment: (1) the holding time between layers was achieved by manually changing the target position with a longer average holding time of about 80 s, compared to 13 s achieved with automated target changeover, and (2) the film had a very low 123 layer thickness of about 6.5 nm. Vertical alignment of nanoparticles in superlattice-type structures is affected by both the layer spacing and the holding time²⁰, with a longer holding time presumably enhancing vertical alignment by allowing the island particles more time to nucleate on energetically disturbed sites. So it is not unexpected that some amount of vertical alignment of particles was observed in these films, but not in all cases. The formation of columnar defects is of interest, as columnar defects are expected to have greater pinning strength than do point defects^{3,4}.

Selected area diffraction patterns confirmed the presence of two distinct phases, consistent with identification as 123 and 211 with orthorhombic structure and slightly varying lattice parameters or similar phase. The selected area diffraction peaks were shifted slightly compared to reference 123 and 211 patterns, suggesting the phases are in relative states of stress or distorted from lattice strains caused by the lattice parameter mismatch. The 123 phase is highly *c*-axis oriented in the superlattice films²¹ and the in-plane orientation of 123 as measured by Phi scans is in general excellent with a full-width half-maximum (FWHM) of about 1.2° .

The effect of the 211 nanoparticle addition on critical current densities is shown in Fig. 3. Transport J_c (J_{ct}) for the composite films are compared to 123 films fabricated by PLD and the BaF_2 process^{12,13}. In particular for applied magnetic field greater than

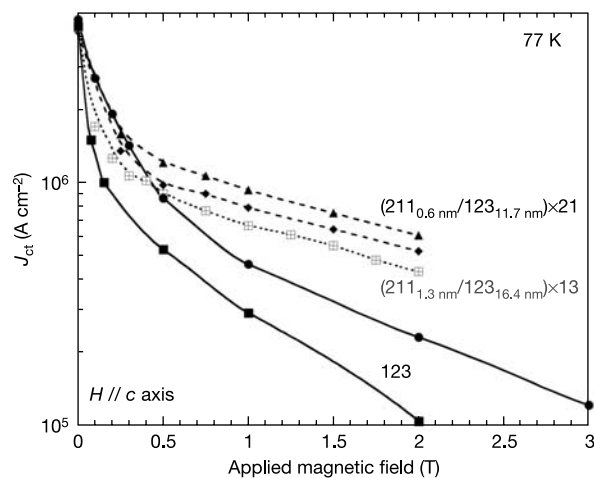


Figure 3 Critical current density as a function of applied magnetic field for YBCO + nanoparticle films compared to pure YBCO films. 123 films (solid lines) were deposited by PLD (filled squares)¹², and recent sample data provided by Oak Ridge National Laboratory of 123 on CeO_2 -coated $\text{Zr}(\sim 9\% \text{Y})\text{O}_2$ substrates (circles) using the BaF_2 process¹³. Multilayer films (dashed lines) were measured for different 211 and 123 parameters, and for samples from the same deposition run (triangles and diamonds). J_{ct} values were measured on bridge-patterned samples by a four-probe transport method with a $1 \mu\text{V cm}^{-1}$ criterion; bridge dimensions were 0.05–0.075 cm wide and 0.3–0.6 cm in length. J_c was calculated using the total film thickness including 211 and 123 layers. The film thickness, bridge widths and dimensions were measured several times to reduce the standard errors of each of these measurements to <5%.

0.3 T, the composite films had a flatter dependence on applied field, and the absolute values of J_c began to increase with respect to 123 films. The self-field J_{ct} of the composite films were increased to above 4 MA cm^{-2} from initial results of $2\text{--}3 \text{ MA cm}^{-2}$ (ref. 21). The increase of the self-field J_c was achieved by decreasing the 211 particle deposition time and hence the 211 'pseudo' layer thickness from 1–1.5 nm to 0.5 nm. A decrease of 211 'pseudo-layer' thickness from 1.0 nm to 0.5 nm increases the volume percentage of the 123 phase and presumably reduces the intrinsic stresses of the 211/123 composites. This decrease in thickness of 211 also increased the T_c from $88.9 \pm 0.2 \text{ K}$ to $90.2 \pm 0.4 \text{ K}$ on average (for a layer thickness of $\sim 11 \text{ nm}$ for 123). These factors combined potentially enhance the zero-field J_c . □

Received 22 April; accepted 28 June 2004; doi:10.1038/nature02792.

1. Bednorz, J. G. & Müller, K. A. Possible high T_c superconductivity in the Ba-La-Cu-O system. *Z. Phys. B* **64**, 189–193 (1986).
2. Wu, M. K. *et al.* Superconductivity at 93 K in a new mixed-phase Y-Ba-Cu-O compound system at ambient pressure. *Phys. Rev. Lett.* **58**, 908–910 (1987).
3. Larbalestier, D., Gurevich, A., Matthew Feldmann, D. & Polyanski, A. High- T_c superconducting materials for electric power applications. *Nature* **414**, 368–377 (2001).
4. Matsushita, T. Flux pinning in superconducting 123 materials. *Supercond. Sci. Technol.* **13**, 730–737 (2000).
5. Civalè, L. *et al.* Vortex confinement by columnar defects in $\text{YBa}_2\text{Cu}_3\text{O}_7$ crystals: enhanced pinning at high fields and temperatures. *Phys. Rev. Lett.* **67**, 648–651 (1991).
6. Selvanickam, V. *et al.* Fabrication of 100 A class, 1 m long coated conductor tapes by metal organic chemical vapor deposition and pulsed laser deposition. *Physica C* **392–396**, 859–862 (2003).
7. Verebelyi, D. T. *et al.* Uniform performance of continuously processed MOD-YBCO-coated conductors using a textured Ni-W substrate. *Supercond. Sci. Technol.* **16**, L19–L22 (2003).
8. Groves, J. R. *et al.* Recent progress in continuously processed IBAD MgO template meters for HTS applications. *Physica C* **382**, 43–47 (2002).
9. Goyal, A. *et al.* Recent progress in the fabrication of high- J_c tapes by epitaxial deposition of YBCO on RABiTS. *Physica C* **357–360**, 903–913 (2001).
10. Balachandran, U. *et al.* Development of coated conductors by inclined substrate deposition. *Physica C* **392–396**, 806–814 (2003).
11. Kakimoto, K., Iijima, Y. & Saitoh, T. Fabrication of long-Y123 coated conductors by a combination of IBAD and PLD. *Physica C* **392–396**, 783–789 (2003).
12. Yamasaki, H., Nakagawa, Y., Sawa, A., Obara, H. & Develos, K. Flux pinning effects of twin boundaries studied with unidirectionally twinned YBCO films. *Physica C* **372–376**, 1885–1889 (2002).
13. Feenstra, R., Christen, D. K., Klabunde, C. E. & Budai, J. D. Role of oxygen vacancies in the flux-pinning mechanism, and hole-doping lattice disorder in high-current-density $\text{YBa}_2\text{Cu}_3\text{O}_{7-x}$ films. *Phys. Rev. B* **45**, 7555–7558 (1993).
14. Larbalestier, D. C. & Maley, M. P. Conductors from superconductors: conventional low-temperature and new high-temperature superconducting conductors. *MRS Bull.* **18**, 50–56 (Aug. 1993).
15. Dam, B. *et al.* Origin of high critical currents in $\text{YBa}_2\text{Cu}_3\text{O}_{7-x}$ superconducting thin films. *Nature* **399**, 439–442 (1999).
16. Pan, V. M. *et al.* Nature of magnetic field and angular dependencies of the critical current density in epitaxial HTS $\text{YBa}_2\text{Cu}_3\text{O}_{7-x}$ films. *Physica C* **388–389**, 431–432 (2003).
17. Reichelt, K. Nucleation and growth of thin films. *Vacuum* **38**, 1083–1099 (1988).
18. Redl, F. X., Murray, K.-S., Cho, C. B. & O'Brien, S. Three-dimensional binary superlattices of magnetic nanocrystals and semiconductor quantum dots. *Nature* **423**, 968–971 (2003).
19. Springholz, G., Holy, V., Pinczolits, M. & Bauer, G. Self-organized growth of three-dimensional quantum-dot crystals with FCC-like stacking and a tunable lattice constant. *Science* **282**, 734–737 (1998).
20. Liu, P., Zhang, Y. W. & Lu, C. Self-organized growth of three-dimensional quantum-dot superlattices. *Appl. Phys. Lett.* **80**, 3910–3912 (2002).
21. Haugan, T. *et al.* Island-growth of Y_2BaCuO_5 nanoparticles in $(211_{-1.5 \text{ nm}}/123_{-10 \text{ nm}})_{\text{XN}}$ composite multilayer structures to enhance flux pinning of $\text{YBa}_2\text{Cu}_3\text{O}_{7-x}$ films. *J. Mater. Res.* **18**, 2618–2623 (2003).
22. Gross, R. E. & Campbell, A. M. Numerical calculation of elastic pinning parameters by point pins. *Physica C* **260**, 188–196 (1996).
23. Haugan, T., Barnes, P. N., Brunke, L., Maartense, I. & Murphy, J. Effect of O_2 partial pressure on $\text{YBa}_2\text{Cu}_3\text{O}_{7-x}$ thin film growth by pulsed laser deposition. *Physica C* **297**, 47–57 (2003).
24. Zhu, Y., Cai, Z. X., Budhani, R. C., Suenaga, M. & Welch, D. O. Structures and effects of radiation damage in cuprate superconductors irradiated with several-hundred-MeV heavy ions. *Phys. Rev. B* **48**, 6436–6450 (1993).

Acknowledgements The Air Force Office of Scientific Research supported this work. We thank J. Murphy, L. Brunke, J. Evans and T. Campbell for experimental assistance, and S. Apt of UES Inc. at the Wright-Patterson AFB Materials Directorate for assistance with SEM and TEM. We also thank R. Feenstra and A. A. Gapud at Oak Ridge National Laboratory (ORNL) for providing $J_c(H)$ data for a reference 123 film.

Competing interests statement The authors declare that they have no competing financial interests.

Correspondence and requests for materials should be addressed to T.J.H. (timothy.haugan@wpafb.af.mil).